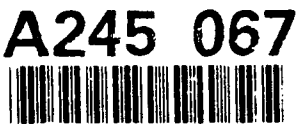

(2)

227000-1-F

Final Report

CONCEPT DESIGN PHASE EXPENDABLE HOLOGRAPHIC SENSOR TO MEASURE OCEAN SMALL ANGLE OPTICAL SCATTERING

FRED J. TANIS

Center for Earth Sciences
Advanced Concepts Division

JULY 1991

ONR CONTRACT NO. N00012-90-C-0091

Dr. Curtis Mobley Code 1123OP
The Office of Naval Research
800 N. Quincy Street
Arlington, VA 22217

ERIM P.O. Box 134001 Ann Arbor, MI 48113-4001

REPORT DOCUMENTATION PAGE

Form Approved
OMB No. 0704-0188

1a REPORT SECURITY CLASSIFICATION UNCLASSIFIED	1b RESTRICTIVE MARKINGS
2a SECURITY CLASSIFICATION AUTHORITY	3 DISTRIBUTION/AVAILABILITY OF REPORT UNLIMITED
2b DECLASSIFICATION/DOWNGRADING SCHEDULE	
4 PERFORMING ORGANIZATION REPORT NUMBERS(S) 227000-1-F	5 MONITORING ORGANIZATION REPORT NUMBER(S) N00012-90-C-0091
6a NAME OF PERFORMING ORGANIZATION Environmental Research Institute of Michigan (ERIM) 6b OFFICE SYMBOL *(if applicable)*	7a NAME OF MONITORING ORGANIZATION Office of Naval Research
6c ADDRESS (City, State, and ZIP Code) P.O. Box 134001 Ann Arbor, MI 48113-4001	7b ADDRESS (City, State, and ZIP Code) 800 N. Quincy Street Arlington, VA 22217
8a NAME OF FUNDING /SPONSORING ORGANIZATION Office of Naval Research 8b OFFICE SYMBOL *(if applicable)*	9 PROCUREMENT INSTRUMENT IDENTIFICATION NUMBER
8c ADDRESS (City, State, and ZIP Code) 800 N. Quincy Street Arlington, VA 22217	10 SOURCE OF FUNDING NUMBERS PROGRAM ELEMENT NO. / PROJECT NO. / TASK NO. / WORK UNIT ACCESSION NO.

11 TITLE (Include Security Classification) Concept Design Phase Expendable Holographic Sensor to Measure Ocean Small Angle Optical Scattering

12 PERSONAL AUTHOR(S) F.J. Tanis

13a TYPE OF REPORT	13b TIME COVERED	14 DATE OF REPORT (Year, Month, Day)	15 PAGE COUNT
Technical	FROM_____TO_____	1991/7/1	60

16 SUPPLEMENTARY NOTATION

17 COSATI CODES			18 SUBJECT TERMS *(Continue on reverse if necessary and identify by block number)*
FIELD	GROUP	SUB-GROUP	

19 ABSTRACT (A preliminary design concept has been developed for a holographic instrument to measure scattering and beam transmission optical properties of ocean waters. The expandable instrument is being developed for use with ship or aircraft deployment using the XDT/AXBT technology. The instrument design has been separated into four measurement functions: (1) beam transmission, (2) small angle scattering, (3) large angle scattering, and (4) backscatter. The present research has focussed on developing and demonstrating a holographic design to measure small angle scattering. This instrument measures the modulation transfer function (MTF) of the particles suspended in the water. The MTF can be inverted with a Fourier-Bessel transform procedure to estimate the volume scattering function at small angles. A laboratory demonstration hologram was constructed to focus a sinusoidal pattern scattered by polystyrene spheres onto a linear detector array. The laboratory results showed loss of contrast with increasing spatial frequency. Simulation model results for a 25cm instrument demonstrated the capability to measure contrast loss at selected spatial frequencies and used that information to derive the volume scattering function for angles from 0.005° to 0.5°.

20 DISTRIBUTION/AVAILABILITY OF ABSTRACT	21 ABSTRACT SECURITY CLASSIFICATION	
☐ UNCLASSIFIED/UNLIMITED ☐ SAME AS RPT ☐ DTIC USERS	UNCLASSIFIED	
22a NAME OF RESPONSIBLE INDIVIDUAL Fred Tanis	22b TELEPHONE (Include Area Code) (313) 994-1200	22c OFFICE SYMBOL

FOREWORD

This is the final technical report for the design feasibility study under Office of Naval Research contract N00014-90-C-0091. This effort has formulated a preliminary design for an expendable instrument to profile the optical properties of ocean waters.

The work reported here was performed by members of the Center for Earth Science, Advanced Concepts Division, Environmental Research Institute of Michigan. Mr. Fred J. Tanis of the Center for Earth Science served as the project Principal Investigator. The Scientific Officer for the Office of Naval Research was Dr. Curtis Mobley, code 11230P.

The support of the Center for Earth Science Staff is gratefully acknowledged, in particular, Mr. Mark A. Endicott, Mr. John Fiaschetti, Mr. Brett Hulett, Mr. Jim Clinthorne, Dr. David Lyzenga, Ms. Janice Anquetil, and Ms. Marsha Neagle. In addition Mr. Juris Upatnieks and Dr. Anthony Tai of the Optical Sciences Laboratory are acknowledged for their contributions to the laboratory experiments.

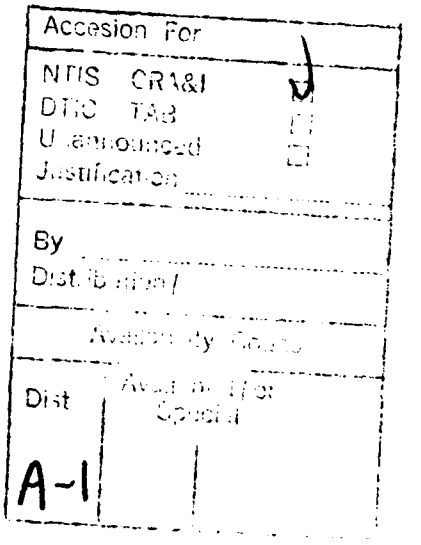

CONTENTS

CONTENTS (CONT.)

FIGURES

FIGURES (CONT.)

FIGURES (CONT.)

TABLE

1.0 EXECUTIVE SUMMARY

A preliminary design concept has been developed for a holographic instrument to measure scattering and beam transmission optical properties of ocean waters. The focus of this design process is an instrument which can be developed into an expendable unit with size constraints imposed by the expendable batho-thermograph/airborne expendable batho-thermograph (XBT/AXBT) technology. The instrument design has been separated into four measurement functions: (1) beam transmission, (2) small angle scattering, (3) large angle scattering, and (4) backscatter. The present research has focussed on developing and demonstrating a holographic design to measure small angle scattering. This instrument measures the modulation transfer function (MTF) of the particles suspended in the water. The MTF can be inverted with a Fourier-Bessel transform procedure to estimate the volume scattering function at small angles. A series of simulation codes were developed to investigate instrument performance. In a laboratory demonstration a hologram was constructed to focus a sinusoidal pattern scattered by polystyrene spheres onto a linear detector array. The laboratory results showed loss of contrast with increasing spatial frequency for particle sizes greater than 1.0 micron diameter. The laboratory observations were consistent with the model simulations both for the small (0.49μm) and large (25.0μm) particles. The simulation model results for a 25cm instrument demonstrated the capability to measure contrast loss at selected spatial frequencies and used that information to derive the volume scattering function for angles from 0.005° to 0.5°. Simulation of the laboratory measurements for 25 micron particles were consistent with unscaled laboratory measurements.

2.0 INTRODUCTION

The objectives of this research are (1) to develop a concept for an expendable optical sensor for ocean transmission and scattering measurements using Holographic Optical Elements (HOEs), (2) to evaluate performance by simulating the instrument measurement properties, and (3) to demonstrate the performance of the HOE in the laboratory, using a known particle size distribution and scattering functions developed from Mie calculations. The first section of the report describes the overall instrument preliminary design which has been partitioned into four measurement functions: beam transmission, small angle scattering ($\theta \leq 10°$), large angle scattering ($10° < \theta < 170°$), and back scattering near 180° ($170° \leq \theta \leq 180°$). For the present study the research was focussed on developing a holographic small angle scattering meter. Following a discussion of the proposed instrument to measure ocean optics is an outline of the theory for small angle scattering measurements. The next section is a description of the laboratory setup. Following are sections describing laboratory and model simulation results. The last section of the report provides guidelines and recommendations for development of a integrated holographic instrument.

2.1 OCEAN OPTICAL INSTRUMENT OVERVIEW

The proposed expendable instrument is being developed for ship and survey aircraft deployment (see Figure 1). The airborne version will be launchable from a standard sonobuoy tube. The submersible instrument will measure inherent optical properties of the ocean which are independent of incident illumination at the surface. The principal inherent properties are absorption (a), beam attenuation (c), and the volume scattering function $\sigma(\theta)$. These properties together specify radiative transfer in the oceanic medium and are interrelated by the following simple expressions.

OPERATIONAL SEQUENCE

1) The Unit is Deployed by Hand Over the Side of Any Ship Without a Launcher or From Aircraft Deployed From a Sonobuoy Launch Tube

2) The Buoy is Activated Electronically Upon Contact With the Water

3) A Carbon Dioxide Cartridge Inflates a Flotation Bag of the Surface Module and Erect and Antenna Within the Bag

4) The Surface Buoy Drifts Away From the Ship Before Releasing the Optical Instrument Thereby Avoiding Ship Shadow and Wake Interference

5) The Optical Data Obtained by the Descending Probe is Converted to Frequency Data and Telemetered Via Signal Wire to the Surface Buoy Where it is Transmitted to the Ship or Aircraft. The Raw Data is Received by a PC Data Logger and Displayed in Real Time as the Probe Descends

6) After the Probe has Completed its Decent, the RF Transmitter is Disabled and the Surface Buoy is Scuttled (Hannon, 1989)

Figure 1. Expendable Instrument Deployment

$$b = 2\pi \int_0^{\pi} \sigma(\theta) \sin\theta d\theta \quad (1)$$

and

$$c = a + b \quad (2)$$

where b is the total scattering coefficient. The current instrument design concept has the capability to measure beam attenuation and the volume scattering function. Use of holographic optics can meet instrument optical performance requirements and provide integration of complex optical components into a compact space with low production cost.

There is Navy need for extensive knowledge of the optical properties of the oceans to predict performance of optical systems operating in the ocean environment and to expand remote observations of the ocean environmental parameters. In addition, there is a science objective to obtain optical closure between attenuation, scattering, and absorption. Oceanic volume scattering functions are highly anisotropic and characteristically have a large forward diffraction peak. Presently there are very few instruments capable of small angle scattering or absorption measurements. Thus, development of a small angle scattering measurement technique and instrument is important to both NAVY science and operational systems objectives for ocean optics.

2.2 HOLOGRAPHIC OPTICAL SYSTEMS

The need for complex optical systems in a compact expendable ocean instrument can be met using holographic optical elements. A hologram is a coded diffraction pattern on a film plate. When a hologram is illuminated with coherent light of the same wavelength as that used in the recording procedure, the object image is reproduced in the object plane. Holograms can be used to satisfy complex optical design requirements which would be impractical to build using conventional lens optics. In the design of a small instrument with complex optics needed for simultaneous measurement of scattering and attenuation, the holographic system is attractive since multiple optical functions can be incorporated into a single hologram.

It is desirable to build an instrument that measures ocean optical parameters in the blue green spectral region and since the current diode technology does not presently provide compact blue-green lasers, other sources were investigated. Thus, the requirement to use a coherent source in a holographic design was examined early in the study. Optical ray tracing models were used to examine the use of an incoherent source, such as a LED, in combination with holographic optics. The results of these studies suggested that this combination would be a highly inefficient means (less than 0.1%) to project a simple beam needed in a transmissometer application. Under ideal conditions holograms can reach efficiencies of ten percent or greater, but only with coherent sources. Presently, inexpensive visible diode lasers are available only in the red (640 and 670nm). The technology is expected to produce inexpensive blue-green lasers within three to five years.

2.3 PROPOSED HOLOGRAPHIC INSTRUMENT CONCEPT

The proposed design for the expendable optical sensor includes four components each which requires specialized holographic design elements. These are: small angle scatterometer (0 - 10 deg.), large angle scatterometer (10 - 170 deg.), backscatter meter (170 - 180 deg.), and the beam transmissometer. Together these instrument components will allow measurement of the beam attenuation coefficient and the volume scattering function. The development of holographic elements for this instrument permits a compact design although the possibility remains that optical cross talk could greatly diminish performance. The basic four components of the proposed instrument are shown in Figure 2.

2.3.1 Small Angle Scattering Meter

The current research has focussed on the development of a small angle meter (see Figure 2a) which measures the MTF. The MTF can in turn be used in combination with the beam attenuation measurement to derive an estimate of the volume scattering function for scattering angles less than ten degrees. In this measurement concept a bar pattern embedded in the hologram is projected through the sample medium either as collimated or focussed light onto a linear detector array which is used to measure the MTF. In this approach it is not necessary to measure the MTF over a wide range of spatial frequencies. Measurements made at critical spatial frequencies are used to parameterize a semi-analytical MTF characteristic of the sample water type. Numerical techniques are used to invert the MTF to estimate small angle scattering components of the volume scattering function.

In the present instrument concept there are several arguments for using the focussed versus collimated light. In the focussed case the interface refraction effects

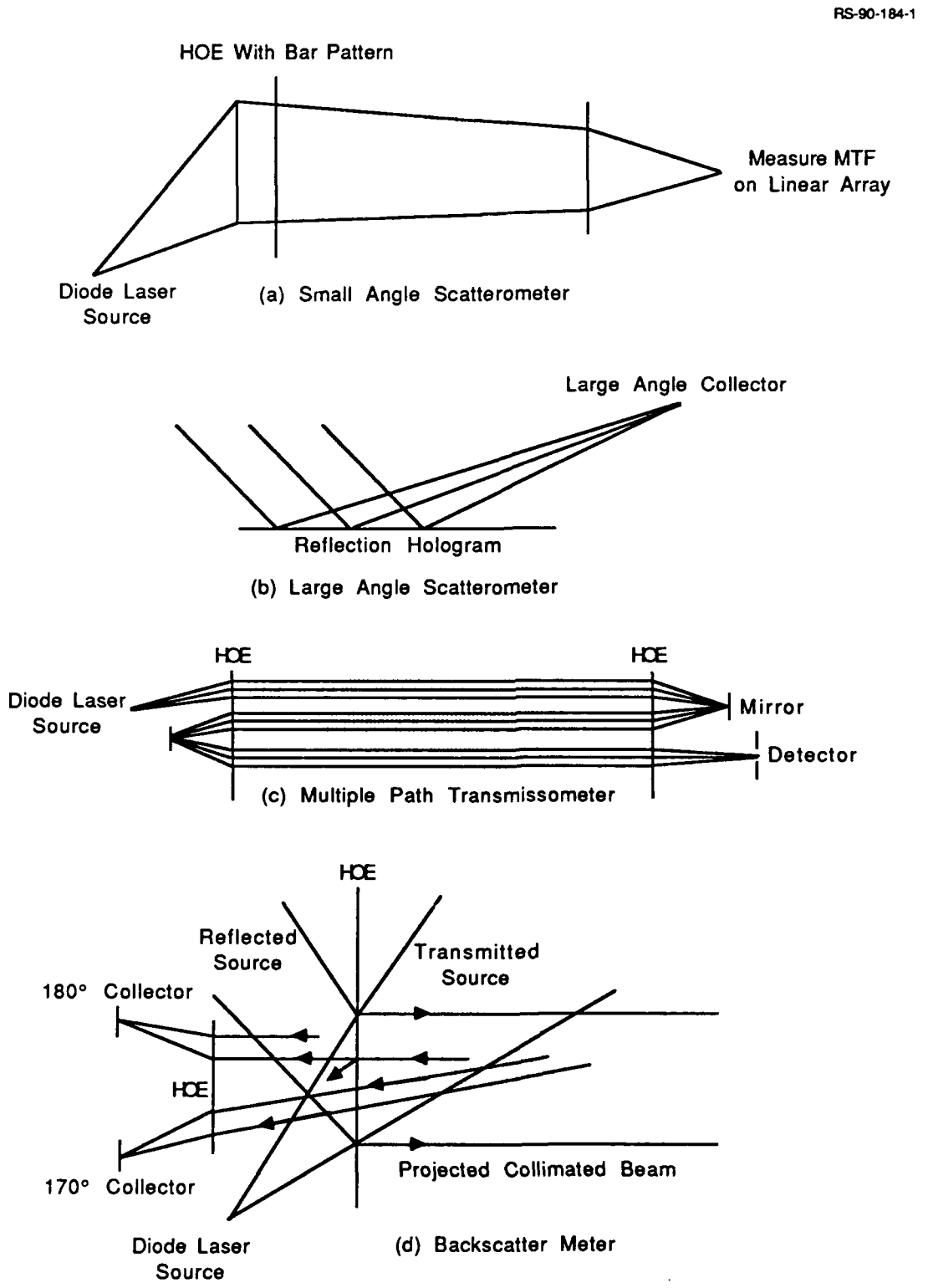

Figure 2. Expendable Scatterometer and Transmissometer Concept

are also recorded on the same hologram and therefore are completely accounted for in the projected beam. Construction of a collimated holographic system is considered more difficult than using focussing techniques. A hologram which projects an image of a slit or bar pattern in prefect collimation along the sample path is very difficult to construct. Furthermore, a second hologram or equivalent cylindrical lens would be required to focus the collimated light effectively onto the linear detector array. In the case of a focussed light and holographic optics, all of the light is efficiently directed to the detector array as is the light scattered in small angles. Problems of stray light are minimized. Other numerical arguments are made in the following sections.

2.3.2 Large Angle Scattering Meter

It is envisioned that the large angle scatterometer (see Figure 2b) will consist of reflection holograms designed as long narrow strips each capable of focussing the incident light received over a narrow range of incident angles to a single detector. The strip holograms can be laid along side one another to form a collector bar having as much as three quarters of the length of the sample volume. Multiple bar reflectance holograms can be developed on the same holographic plate. It is envisioned that the bar holograms could be incorporated into the open connecting framework that surrounds the sample volume.

2.3.3 Beam Transmissometer

The beam attenuation coefficient is linear with mass or volume if the particle size distribution and absorption characteristics are constant. In a beam attenuation meter a point source of light is placed at the focal point of a thin lens forming a collimated beam of light. The beam passes through the sample to a second lens which focusses

the collimated beam onto a small detector placed at the focal point. Any light that is absorb by the medium is lost. Light that is scattered from the beam does not focus on the detector. Thus, over the sample path, light received by the detector measure the total beam attenuation.

The design path length for making beam transmission measurements in the blue-green region should be at least one meter in length to obtain a one percent accuracy for the beam attenuation coefficient. Thus, in an expendable transmissometer design the collimated beam must be folded and passed a number of times through the sample medium. Our proposed design is based on passing such a narrow collimated beam back and forth between two holograms each containing the properly designed lenslet array. Although the diagram in Figure 2c shows three passes, the transmissometer design will have a minimum of four passes and a maximum of eight. For a large number of passes interface losses will prevent accurate measurements. Development of a lenslet array is ideal since one can precisely and easily locate the optics within the integrated HOE. In the design the primary hologram will be used to form a collimated beam which is passed through the sample medium to a second HOE. The beam is then focussed onto a small plane mirror and pin-hole. The beam is reflected to another lens of the array which re-collimates the remaining light for transmission along the return path. With proper design of these optics much of the error in the attenuation coefficient due to small angle scattering is eliminated. We propose to generate this holographic pair of lenslet arrays and demonstrate transmissometer performance in the laboratory.

2.3.4 Backscatter Meter

The backscatter meter design is shown as Figure 2d. In the instrument concept design this device will be positioned behind the initial beam forming lens in the

transmissometer HOE. As shown in Figure 2d a portion of the incident source beam on the hologram is transmitted, a portion reflected, and a portion transmitted as a collimated beam. The light backscattered at angles near 180 degrees will be transmitted through the hologram with approximately 50% being directed back toward the source and 50% unaltered in direction. This latter portion can be diffracted in a second hologram to separate detectors depending on the original scattering angle in sample volume.

2.3.5 Edge Illuminated HOEs

The HOEs needed in backscatter meter and beam transmissometer could be highly efficient and at the same time compact by using edge illuminated HOEs. The diffraction efficiency of these elements can be made nearly 100% for polarized light. In this design, light emerging from the HOE becomes the collimated beam needed for the transmissometer. As above, 50% of the unpolarized backscattered light is directed to a second HOE which is similar to the first but at right angles to the first so as to efficiently diffract the light to a detector. The advantage of using edge-illuminated HOEs is that they are monolithic and therefore avoid air-glass interface problems (Upatnieks, 1988).

3.0 SMALL ANGLE SCATTERING THEORY

The fundamental description of light scattering by particles in sea water is the volume scattering function, $\sigma(\theta)d\omega$, which is defined as the amount of light scattered per meter into a differential solid angle in a specific direction. For single scattered light an instrument can be designed to collect the light at a specific angle such as the Austin and Petzold [1975] ALSCAT instrument. The problem is getting reliable measurements at very small angles needed to define the diffraction peak where the physical limits prevent fixed angle measurements. Multiple scattering at these small angle may also contribute to significant errors. While measurements made with the ALSCAT instrument have been used extensively, and in this study, to estimate the entire volume scattering function there are very few measurements available for the world oceans. At small angles the scattering function has typically a very large forward peak resulting from (1) diffraction of light around particles with diameters larger than the wavelength and (2) refraction in particles with a nearly water matching refractive index. In this study the inherent optical parameters refer exclusive scattering by particles. Thus,

$$c_p=a_p+b_p \tag{3}$$

and

$$b=b_w+b_p \tag{4}$$

where b_w is the scattering coefficient for pure sea water.

3.1 MODULATION TRANSFER FUNCTIONS

In the case of significant multiple scattering one must either derive the point spread function (PSF), (f(θ,r)), or the MTF (F(ψ,r)) to gain information on small angle scattering. The MTF describes the loss of contrast as a function of spatial frequency or the loss of contrast as a sinusoidal bar chart. The small angle scattering essentially fills in the vacant spaces between the individual bars. The number of cycles per unit length in the chart, υ relates to the angular spatial frequency, ψ (cyc/radian), by the distance r (i.e., $\psi = \upsilon r$).

The PSFs and the MTFs are integrated by the two dimensional fourier transform. Both of these functions are circular symmetric and can be written, as above, in terms of the distance r along the beam and off axis angle θ. The two dimensional Fourier transform of a circular symmetric function reduces to a one dimensional Fourier-Bessel integral.

$$f(\theta, r) = 2\pi \int_0^\infty J_o(2\pi\theta\psi)\, F(\psi, r)\, \psi\, d\psi \qquad (5)$$

$$F(\psi, r) = 2\pi \int_0^\infty J_o(2\pi\theta\psi)\, f(\theta, r)\, \theta\, d\theta \qquad (6)$$

The small angle approximation has been used in the second integral.

3.2 SMALL ANGLE SCATTERING TRANSFORMS

Since the PSF is a function of the propagation distance r and the scattering angle it cannot be directly related to the volume scattering function. However, Wells [1969, 1972] has shown a transform that allows one to derive $\sigma(\theta)$ from the MTF or

vice versa. Del Grosso [1975] used this technique to measure the MTF for polydispersed particle size distribution. The MTF may be described in terms of a decay function $D(\psi)$ which is independent of measurement distance.

$$F(\psi, r) = e^{-D(\psi) r} \tag{7}$$

$$D(\psi) = -r^{-1} Log_e F(\psi, r) \tag{8}$$

The PSF can result from two types of propagation, focussed or collimated light. It is therefore appropriate to think in terms of two different decay functions; one for focussed light and one for collimated light. The collimated decay function $D_c(\psi)$ can be directly related to the Fourier Bessel transform of $\sigma(\theta)$, $H(\psi)$.

$$H(\psi) = 2\pi \int_0^\infty J_o(2\pi\theta\psi)\, \sigma(\theta)\, \theta d\theta \tag{9}$$

The function $H(\psi)$ is the MTF of the scattering function. Although only values of $\sigma(\theta)$ for $\theta \leq 10^\circ$ effectively contribute to $H(\psi)$ the integration must be carried further to avoid the problems of truncation and produce a satisfactory numerical integration. If $\sigma(\theta)$ has been normalized such that

$$\sigma(\theta) = b_p \sigma_n(\theta) \tag{10}$$

and

$$1=2\pi\int_0^{\pi}\sigma_n(\theta)\sin\theta d\theta \qquad (11)$$

then $1\text{-}H_n(\psi)$ describes the contributing effects of scattering to contrast decay in a bar pattern with spatial frequency. At very large values of ψ all bar patterns are completely obscured by small angle scattering within a very short propagation distance and at the upper limit, $\psi = \infty$ and $1\text{-}H(\psi)=1$. At the low frequency limit ($\psi = 0$) scattering produces no loss (i.e., $1\text{-}H_n(0)=0$). The function

$$D_c(\psi)=a_p+b_p[1-H_n(\psi)] \qquad (12)$$

describes decay of spatial frequencies for collimated light for a distribution of particles with a scattering coefficient of b_p and normalized scattering function $\sigma_n(\theta)$. $D_c(\psi)$ can be used to derive the normalized volume scattering function.

$$\sigma_n(\theta)=2\pi\int_0^{\infty}J_o(2\pi\theta\psi)H_n(\psi)\psi d\psi \qquad (13)$$

For the case of a focussed spatial decay function $D_f(\psi)$ the $D_c(\psi)$ function is integrated over the $[0,\psi]$ interval with the dummy variable u to give a larger value of decay demonstrating the reduced effect of scatters near the focal point

$$D_f(\psi) = \psi^{-1} \int_0^{\psi} D_c(u)\, du \qquad (14)$$

The reverse transform is simply

$$D_c(\psi) = \frac{d[\psi D_f(\psi)]}{d\psi} \qquad (15)$$

One can also think of an equivalent relationship in the θ domain. Since the Fourier-Bessel transform of $d[\psi H(\psi)]/d\psi$ is $-d[\theta\sigma(\theta)]/d\theta$ one can derive the effective scattering function for focussed light, $\sigma_f(\theta)$. From the above relationships it is apparent that

$$H_c(\psi) = \frac{d[\psi H_f(\psi)]}{d\psi} \qquad (16)$$

and

$$\frac{d[\theta\sigma_f(\theta)]}{d\theta} = -2\pi \int_0^{\infty} J_o(2\pi\theta\psi)\, H_c(\psi)\, \psi\, d\psi \qquad (17)$$

implying

$$\sigma_c(\theta) = \frac{-d[\theta\sigma_f(\theta)]}{d\theta} \qquad (18)$$

and

$$\sigma_f(\theta) = \theta^{-1} \int_{\theta}^{\pi} \sigma_c(u)\, du \qquad (19)$$

The physical interpretation of this result is simply for the collimated case light that is scattered at the same angle along the beam will lie at the same position in the PSF $f_c(\theta,r)$ whereas in the focussed case light scattered at the same angle will end up in different locations or conversely light received at a single position on $f_f(\theta,r)$ will have come from angle θ and greater angles. Thus, $\sigma_f(\theta)$ represents the average value of $\sigma_c(\theta)$ over the interval (θ,π).

Thus an alternative and equivalent transform for the focussed case gives $D_f(\psi)$ from $\sigma_f(\theta)$ which is obtained form $\sigma_c(\theta)$ using equation (18). The focussed decay transform for $D_f(\psi)$ becomes

$$D_f(\psi) = C_p - 2\pi \int_{o}^{\infty} J_o(2\pi\theta\psi)\, \sigma_f(\theta)\, \theta d\theta \qquad (20)$$

and the inverse transform

$$\sigma_f(\theta) = 2\pi \int_{o}^{\infty} J_o(2\pi\theta\psi)\, [D_f(\psi) - C_p]\, \psi d\psi \qquad (21)$$

Use of the latter equation will tend to reduce noise in estimating the $\sigma_f(\theta)$ since one avoids introduction of numerical noise in the differentiation step needed in the earlier transform.

3.3 COMPUTATIONAL TECHNIQUES

The small angle scattering analysis procedures are shown in the block diagram of Figure 3. Three basic analysis procedures were followed leading to a derived small angle scattering function. (1) In the laboratory experiments data were collected on a linear detector array and used to estimate contrast loss at selected spatial frequencies. These measurement data were then used to estimate the medium MTF and finally information on small angle scattering. (2) A parallel analysis was conducted starting with the particle size for the laboratory experiment and using Mie theory to estimate the volume scattering function (VSF). The VSF was used in an instrument model to simulate the laboratory measurements. The VSF was transformed to the MTF. The estimated MTF was then compared to the laboratory measurements and simulated measurements. (3) A VSF based upon measurement data was used to calculate the MTF. Instrument size parameters were then used in the model to simulate measured contrast. These measurements were then compared to the MTF derived from VSF and furthermore were used to derive an estimate of the MTF. The inverse transform was then applied to derive the small angle portion of the VSF. Three basic computer codes were developed to simulate the processes for a holographic small angle scattering meter. The combination of codes allows end to end measurement analysis of the volume scattering function.

A code was developed to make the Fourier-Bessel integration transform calculations described above. This code, MTF_SCAT, uses an 8000 point Labatto quadrature in the Fourier-Bessel subroutine and cubic splines in estimating the local derivative. This procedure provides both forward (VSF to MTF) and inverse calculations (MTF to VSF). Equi-space sampling in the log domain was selected since both functions are strongly peak at the origin. The VSF developed for clear ocean water and used in these analyses was based upon Petzold's [1972] scattering

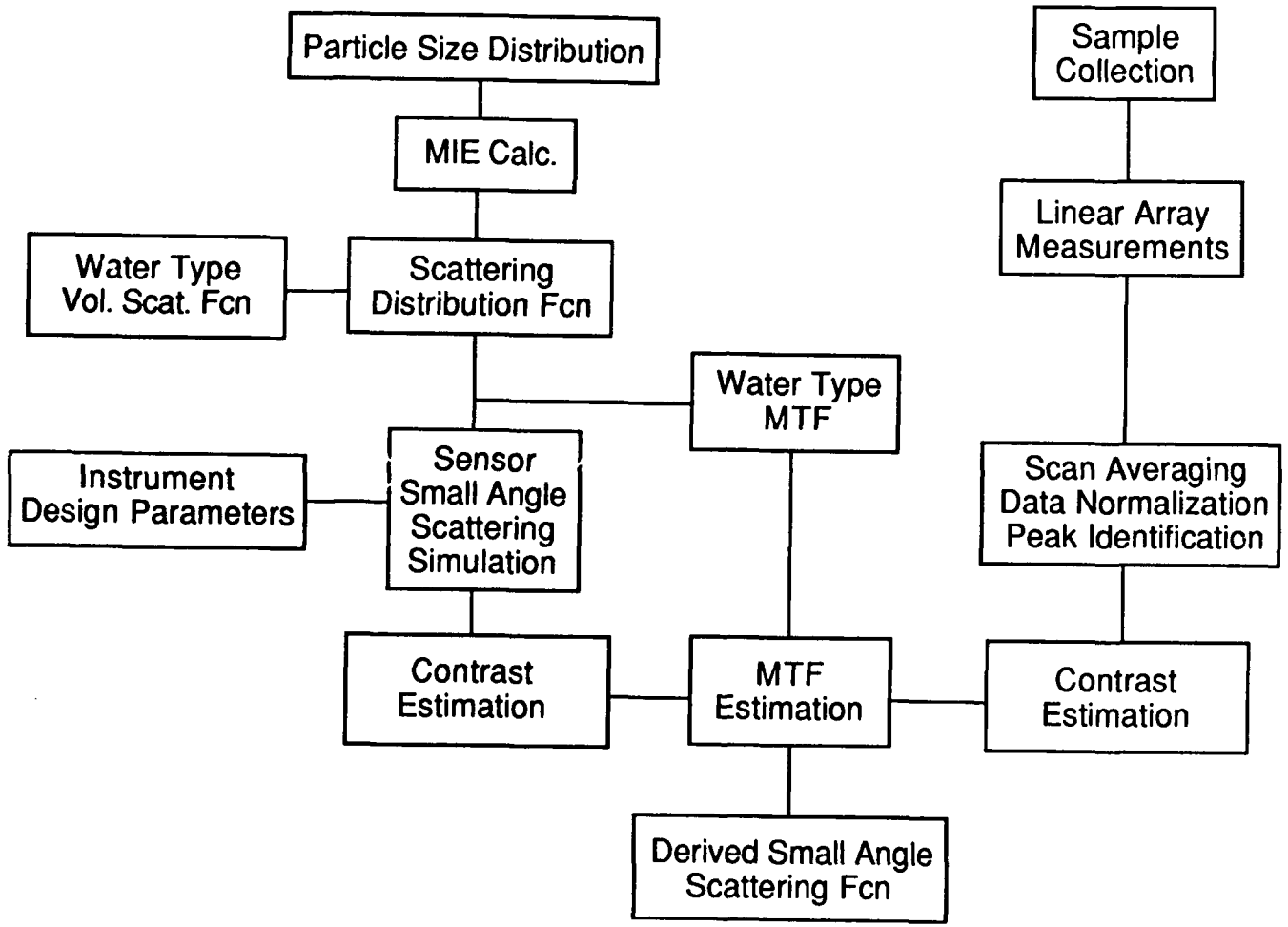

Figure 3. Small Angle Scattering Analysis Procedures

data at 530nm collected for the Tongue of the Ocean. The measured value of attenuation for this sample was $0.199m^{-1}$ and the total scattering coefficient was estimated to be $0.177m^{-1}$. These data were fitted [Tanis et. al., 1986] to a smooth VSF, as shown in Figure 4, using Pede splines. In the MTF calculations the VSF was retained for angles less than 100°. At larger angles the VSF was tapered to zero and the entire modified function was renormalized. This procedure provides a smooth function necessary for the Fourier-Bessel transform calculations. While it is realized that only forward scattering ($\theta < 10°$) is important to the observed MTF a smooth truncation must be provided to minimize truncation effects which are more apparent in the inverse calculations. The derived MTF for the AUTEC sample is shown in Figure 5.

The second code developed, PROBE, is a Monte Carlo model with fixed spatial frequencies designed to simulate the measurement instrument by projecting a bar pattern through the scattering medium and focussing the pattern modified by small angle scattering on to a linear detector array. The approach taken was to force collisions within the sample medium to avoid counting those which escaped. The fraction of photons escaping the first collision and passing through the medium is $e^{-\tau_s}$, where τ_s is the optical thickness of the medium. One forces a collision by sampling from the density function.

$$p(\tau)\, d\tau = \frac{e^{-\tau} d\tau}{(1-e^{-\tau_s})} \qquad (22)$$

The potential bias is handled by multiplying a weight by $1-e^{-\tau_s}$ which yields the fraction of photons remaining in the packet. The weight is reduced at each collision until it falls below a cutoff. At this time a new photon is started in the simulation.

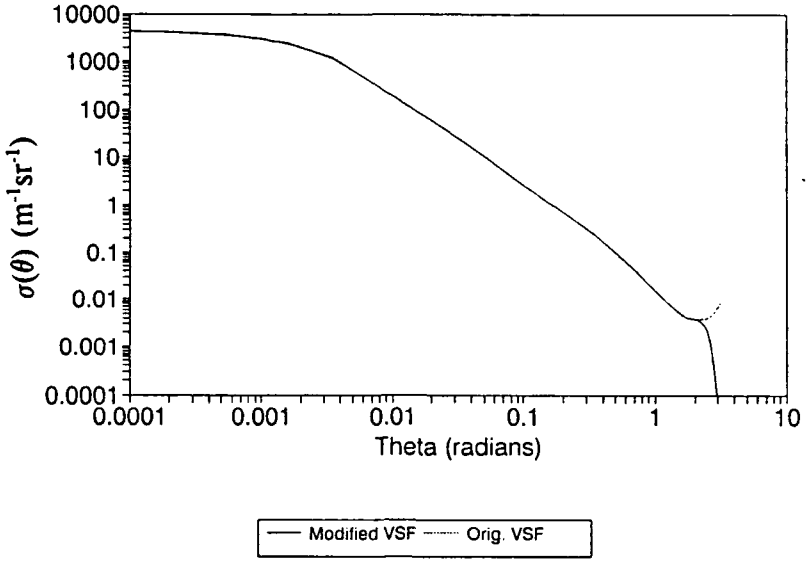

Figure 4. Modified Volume Scattering Function for AUTEC Sample Number 7 and Original Fitted Curve Using Petzold's Measurement Data [1972]

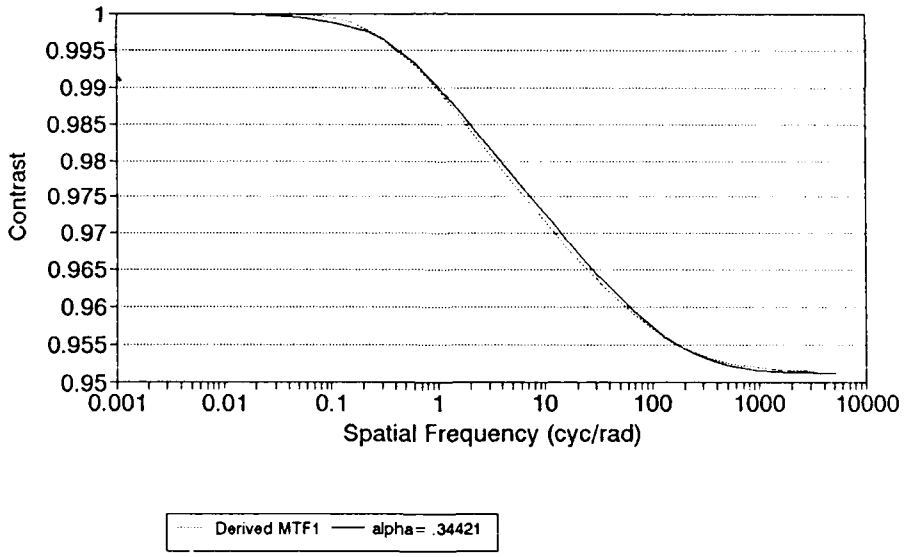

Figure 5. Modulation Transfer Function for AUTEC Sample With Path Length of 25 cm. Also Shown is the Fitted MTF (Solid Curve) With $\alpha = 0.3442$, $\beta = .2428$, $\zeta = 0.39$, and $\gamma = 1.00$

Model scattering includes both Rayleigh and Mie although for the present study only Mie calculations were made.

The spatial distribution of photons leaving the hologram was uniform since every position in the hologram contributes light to the image. The selection of photon initial direction was based upon the distribution of unscattered photons in the image plane as calculated from the sinusoidal bar pattern (see Figure 6). The bar pattern selected was consistent with that chosen for the laboratory experiments and consists of 1024 detector elements (as in the actual linear array). The extensions on either side of the central pattern provide calibration in the contrast calculations and help to prevent humping of the scattered portion due to apparent unequal lateral scattering. For a photon focussed on the end detector only energy scattered in one direction along the array will be recorded whereas in the center recording will be made in both directions.

In the 25cm instrument simulations the hologram was 4.0 x 4.0cm, the detector array size at image focus was 0.04 X 10.24cm. It was assumed that optics were present, as in the laboratory experiments, to re-focus the bar pattern onto an actual array (.01 X 2.56cm). These latter optics were not part of the present simulations. Examples of the scattered portion for a 25cm path length instrument using the AUTEC No.7 volume scattering function are shown in Figure 7 for sample runs of 200, 2500, and 7500 photons. Near convergence is achieved at N_p =2500 for AUTEC No.7 and is sufficient to study the behavior of scattered energy in the present study. More rapid convergence was observed for other volume scattering functions with a smaller diffraction peak. The simulator is completely parameterize to allow the user to set up any instrument geometry, projected pattern, or scattering conditions.

A third code contained three procedures; (1) to derive a semi-analytic fit to the calculated MTF, (2) to generate a series of MTF's based upon a single parameter

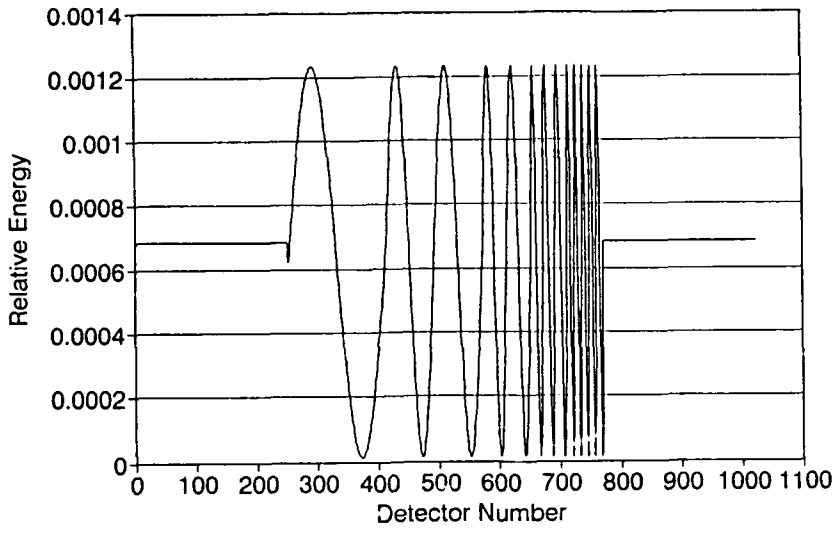

Figure 6. Simulated Unscattered Energy on the Linear Detector Array for a Path Length of 25 cm and Beam Attenuation of 0.2 m^{-1}

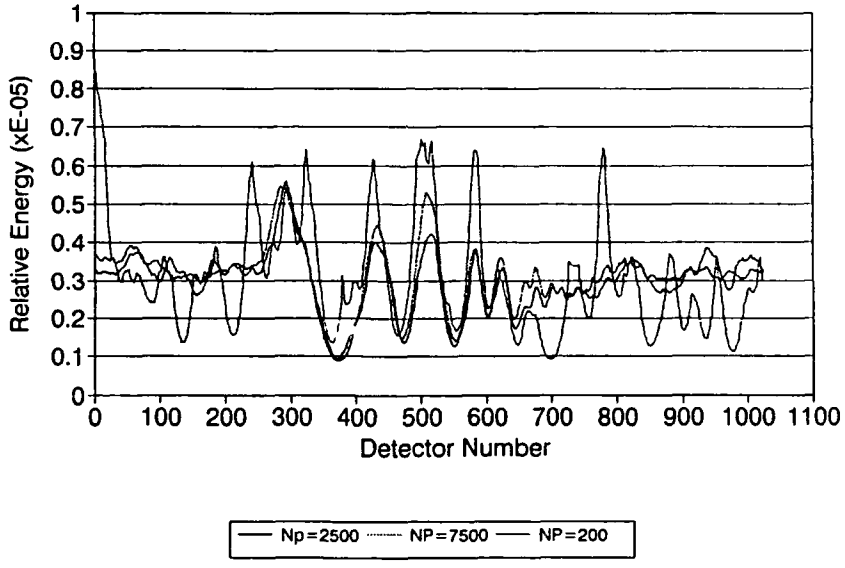

Figure 7. Comparison of Simulated Scattered Energy on Linear Detector Array Using 200, 2500, and 7500 Photons

input, α, and (3) to calculate the best fit based upon measurement data. The MTF curve fitting technique involves fitting two exponential functions which are then splined together. The first function $f_1(\psi)$ is a fit to the MTF at low spatial frequencies.

$$f_1(\psi) = (1-e^{-\tau})\, e^{-\beta\psi^{\gamma}} + e^{-\tau} \tag{23}$$

where τ is the product of path length and c, ψ is spatial frequency in cycles per radian, and γ is a smoothing constant. The function f_1 equals 1 at (ψ=0) and $e^{-\tau}$ at large spatial frequencies. The second function $f_2(\psi)$ has the same formulation as the first and describes the MTF at large spatial frequencies.

$$f_2(\psi) = (1-e^{-\tau})\, e^{-\alpha\psi^{\zeta}} + e^{-\tau} \tag{24}$$

where ς is a smoothing constant for the second function. The function f_2 converges to $e^{-\tau}$ for large values and 1 equals at $\psi = 0$.

Initially both functions are estimated using a known τ and a MTF characteristic of the water type, i.e, one must assume a water type and scattering function to get a characteristic MTF. The two functions are combined into a smooth composite function with spline functions. An example fit is shown in Figure 5 for an α = 0.3442 and β = .2428. An RMS error of $5.1X10^{-4}$ was calculated for this fit. Either function can be changed slightly and the two functions then reconnected. For MTF fitting routine the f_1 function is assumed constant for spatial frequencies less than a few tenths of a cycle/radian. The f_2 function is allowed to vary using only the α parameter. Example MTFs are shown in Figure 8 for the AUTEC sample and a τ

value of 1. These three MTF's were then inverted as shown in Figure 9 to indicate the corresponding variability in small angle VSF at angles less than 0.4 degrees. Also shown is the original AUTEC VSF which compares well with the inverted functions at large angles. The noise observed at angles greater than one radian is an artifact of the Bessel function transform.

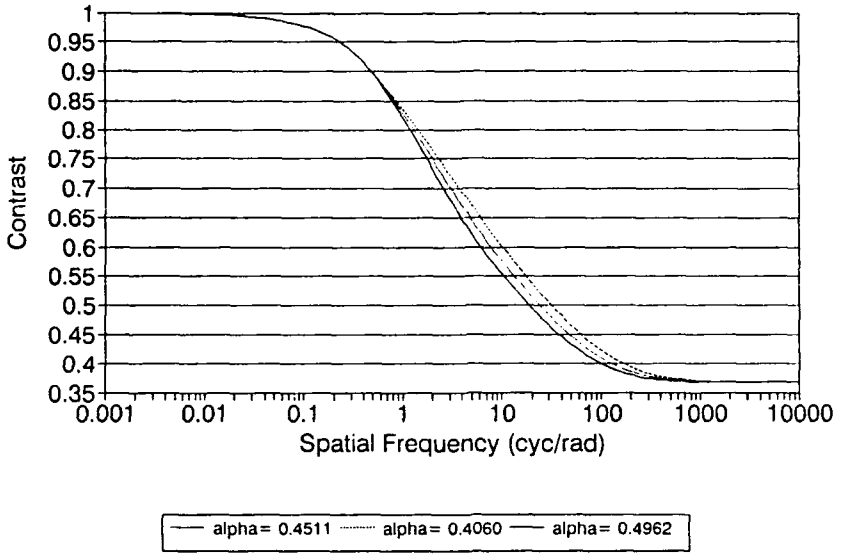

Figure 8. Modulation Transfer Functions Obtained for Selected Values of Alpha

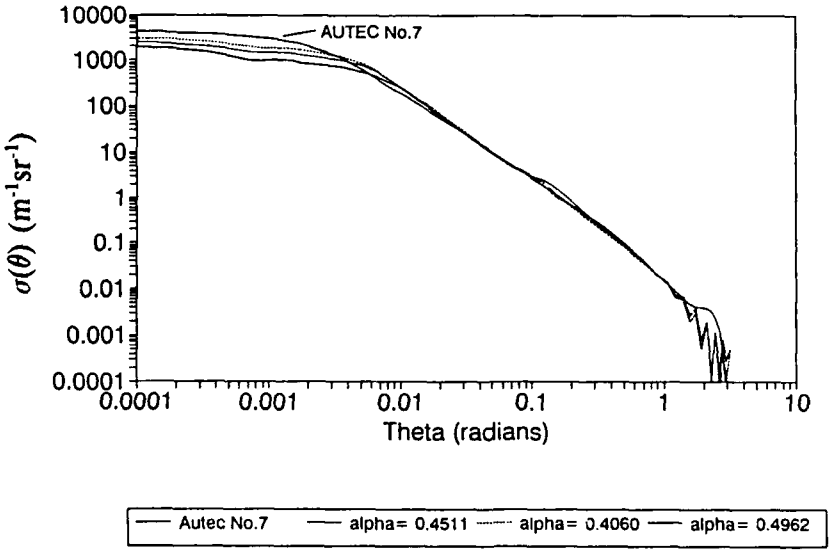

Figure 9. Volume Scattering Functions Derived for the Three MTF s

4.0 LABORATORY METHODS

An experimental setup was assembled to use both methods in the recording of the hologram and also for pattern projection. The laboratory laser table setups are shown as Figures 10 and 11 respectively. The primary laser was a Spectra Physics 125 HeNe laser with 90 to 100mW output and was used to record and play back the hologram (see Figure 12). A second 10mW laser was used to measure particle attenuation in the sample tank (see Figure 13).

4.1 HOLOGRAM RECORDING SETUP

The hologram recording material was 2"X2" Kodak Spectroscopic plates with photo sensitive backing. As shown in Figure 10 the beam was split with the aid of a variable spitter into a beam to illuminate the bar transparency through the water filled tank and a second to create the interference pattern on the recording plate. The plexiglass tank had inside dimensions of 25 by 100 cm and was constructed of 3/8" clear plexiglass. Scattering within the plexiglass sheet was not considered a problem. For hologram recording the tank was filled with nearly 50 liters of filtered deionized/distilled water made available from ERIM's Electronics Facility.

4.2 LABORATORY OPTICAL SYSTEM FOR MEASUREMENTS

In the process of recording the sinusoidal bar pattern all surface refraction effects are included. A field lens was used to gather the light at the image plane and pass it to the linear array via an imaging lens. The linear detector array was an EG&G model RL 1024K unit with 1024 element with center spacing of 25 microns and a length of 100 microns. The bar pattern and optics were sized to efficiently image the

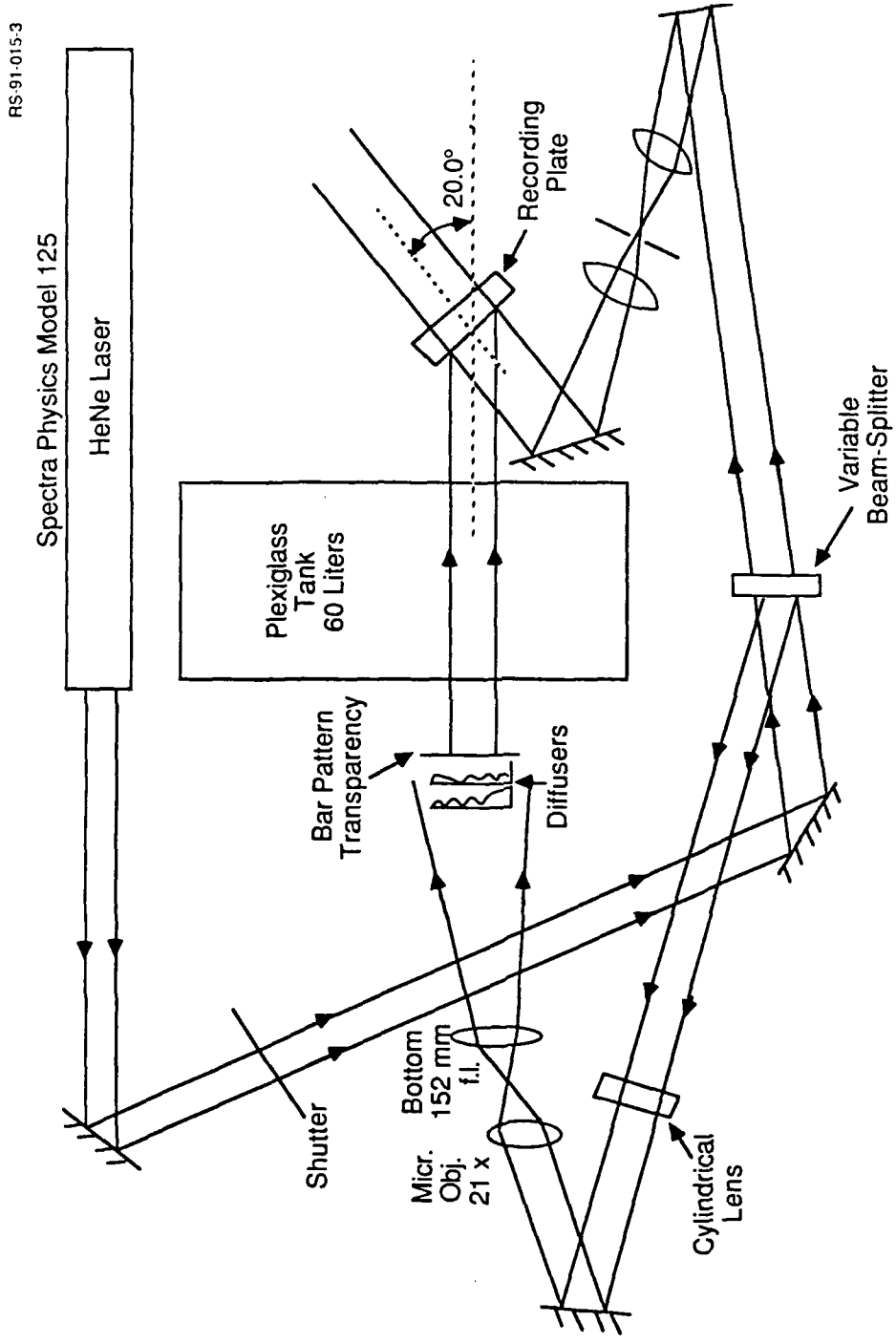

Figure 10. Optical System for Hologram Recording

CES-91-015-2

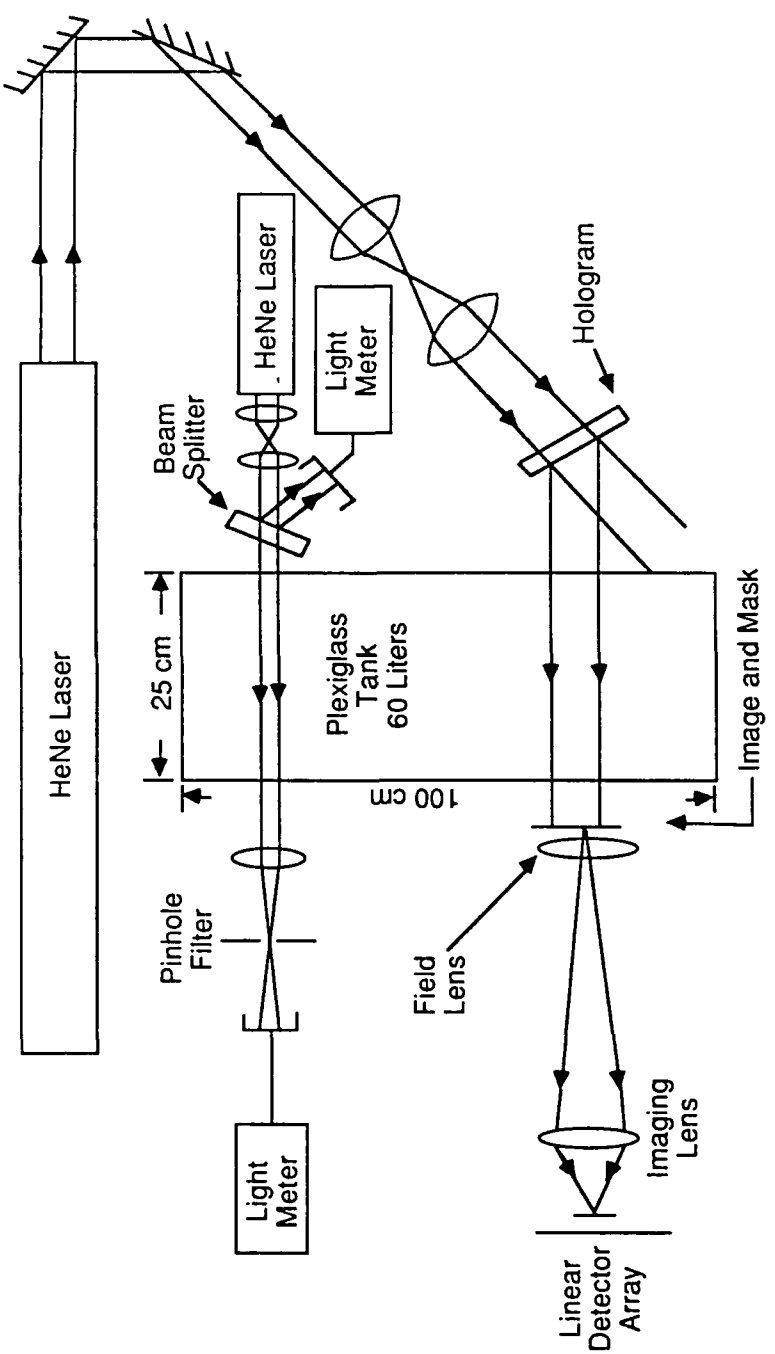

Figure 11. Optical System for Light Scattering Measurement

Figure 12. Hologram With Laser Components (Photograph)

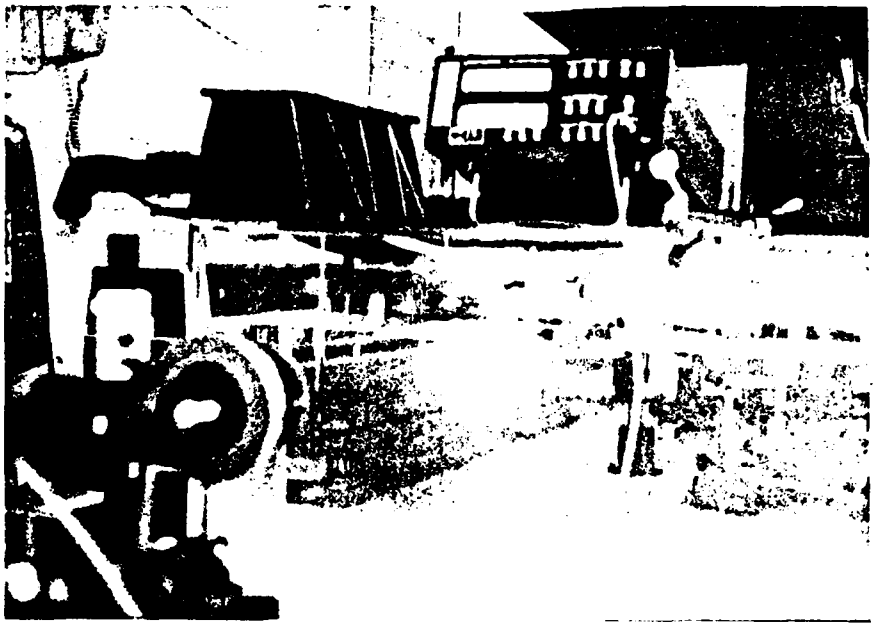

Figure 13. Water Tank and Beam Transmission Measurement (Photograph)

pattern through the tank and onto the linear array. The detected energy on the linear array was sampled using an array dump routine placed on the DSP56 signal processing board. The array data were digitized and passed to a 286 PC for display and data analysis. A flow chart of the data recording system is shown in Figure 14. PC software (LINEAR1K) was developed to provided display of the scan profile at two different magnifications. Data were recorded with sixteen bits of dynamic range. Electronic noise alone reduced measurement significance to about fourteen data bits. Each array scan integrated the detected light energy over a 10 ms period. Multiple scans were then averaged in the PC data acquisition software to reduce electronic and other systematic sources of noise. When data profiles were averaged over 400 scans about 11 data bits were found to be significant. This precision was considered to be adequate to record the dynamic range of the projected bar pattern. Some drift in the system was observed so that noise reduction by averaging had little consequence for collections involving more than 400 scans.

4.3 SINUSOIDAL PATTERN

The sinusoidal bar patterns were computer generated and transferred to film using a high resolution image filming recorder. The spatial frequencies selected were designed for the 25 cm path length and to characterize the portion of the MTF sensitive to small angle scattering. The spatial frequencies of this pattern depend on the distance between hologram and image plane. The path between the hologram and image plane, in the laboratory, was found to be 41 cm including the 25 cm water path and two plexiglas sheets. The resulting spatial frequencies are given in Table 1 with units of cycles per radian.

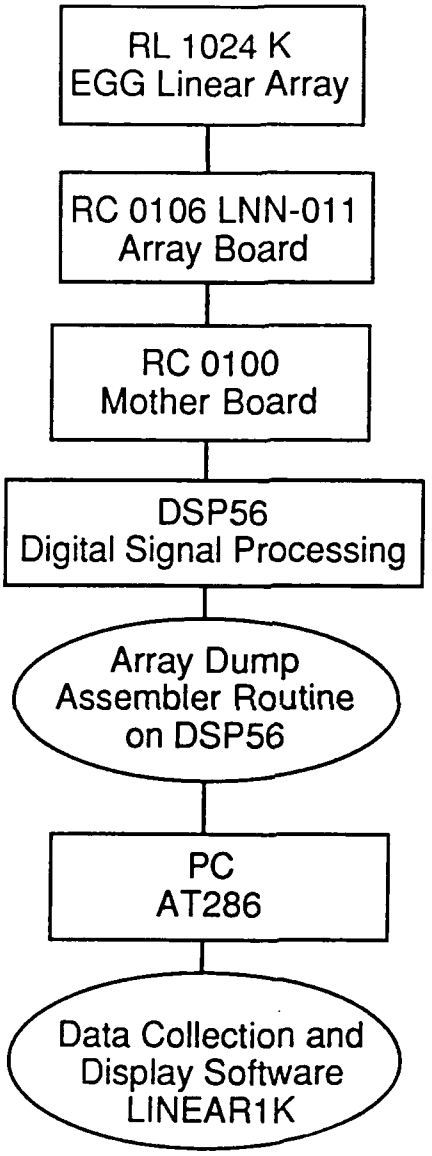

Figure 14. Laboratory Data Recording System

Table 1.

Bar Pattern Spatial Frequencies

Frequency (cyc/rad)	Number of Cycles
25.6	1
51.3	2
102.5	2
205.0	3
341.5	5

4.4 SCATTERING MEDIUM

The tank was seeded with polystyrene spheres available from Polyscience Inc. under the trade name POLYBEAD. The concentration of spheres was diluted into two fractions with concentrations of 1.1×10^9 and 1.1×10^8 particles per milliter. Aliquots from these dilutions were then transferred to the tank which contained 47.5 liters of water. The spheres are considered non-absorbing and have a nominal refractive index of 1.60+0i.

4.5 HOLOGRAM SNR AND DYNAMIC RANGE

Several holograms were developed for this experiment with the objective being to create a hologram with high efficiency and low signal to noise ratio (SNR). Performance characteristics of several of these holograms were measured in the laboratory. Minimum SNR was perhaps of greater importance than maximum

efficiency since an early decision was made to use the large HeNe laser for hologram construction.

The dynamic range of the input bar pattern recorded on the hologram was 10^4:1. It was expected that the resulting hologram would produce a dynamic signal range, in the projected image, in excess of 10^3:1. This range was needed to accurately measure changes in contrast between the light and dark fields due to particle scattering. The best measured dynamic range between the light and dark image fields without the tank and scattering medium was 600:1. When the hologram was mounted for playback through the tank this number was reduced to 100:1. The former range is indicative of the inherent SNR of the hologram due to speckle. The speckle size was estimated to be 6.6 microns square at the HeNe 633nm wavelength. The number of speckles located in one detector element at the image plane was estimated to be $2.3X10^3$. Thus, a measure of the speckle SNR of the hologram is approximately 48:1 which is indicative of the signal standard deviation for a uniform light field. The 600:1 ratio is indicative of the dynamic range of the hologram where the minimum is due largely to speckle. The reduction in this ratio through the tank and water medium is due to both scattering in the water and reception of stray light into the detector field. The speckle noise is a feature of the hologram itself so that if the structure remains fixed the noise limit for a large number of samples will approach some other smaller limit. For the present experiment this lower limit is determined by the number of significant bits in the resulting measurements (approximately 11). The signal due to scattering and its modulation by the sinusoidal pattern were estimated to be 1% to 10% of the dark field signal. With careful control of stray light and the speckle problem, SNRs of 10^3:1 should be achievable.

5.0 EXPERIMENTAL AND SIMULATION RESULTS

The laboratory experiments were intended to demonstrate the holographic technique and cannot be considered quantitative. The instrument scattering model was used for two purposes. First, to simulate contrast loss in a sinusoidal pattern for specific monodispersions of polystyrene spheres used in the laboratory experiments and second, to demonstrate capability of the proposed 25cm instrument to measure small angle scattering. In the second effort contrast loss was simulated from the model knowing the scattering phase function for a polydispersion of ocean particles. These contrasts were then used to estimate a contrast decay function at selected spatial frequencies. A numerical minimum square error procedure was used to estimate the MTF based upon these selected spatial frequencies. The derived MTF was then inverted using Fourier-Bessel transforms to estimate the small angle portion of the volume scattering function.

5.1 POLYSTYRENE SPHERE SEEDING EXPERIMENTS

A seeding experiments were conducted for four particle diameters: 0.049μm, 0.99μm, 2.92μm and 25.0μm. In each of these experiments polystyrene spheres were mixed with ERIM distilled water in five or six steps resulting in a wide range of particle concentrations. A average scan profile recorded on the detector array is shown in Figure 15. All but the first cycle of the pattern is shown which could not be included in the focussed image. The reduced peak size at higher frequencies is an artifact of the photographic and hologram recording processes and could not be avoided. The dynamic range of the detector was maximized for these observations and was far in excess of hologram and stray light noise.

The average background attenuation at 633nm was estimated to be 0.320 m-1. The accepted value at 665nm is 0.364 m-1 [Zaneveld,1984]. The range in the attenuation coefficient for these experiments ranged from 0.32 to 1.0 m^{-1}. Beam attenuation measurements for the 2.92 micron polystyrene spheres is shown in Figure 16.

Calculated contrasts are plotted in Figures 17 and 18 for the observed spatial frequencies and attenuation values. The 25μm diameter spheres showed the largest reduction in contrast of approximately 0.02 from the smallest to largest frequency. For the 0.49μm spheres contrast reduction was minimal. The results from the 0.99μm diameter experiments were noisy and inconclusive. The measurement series with the 2.92μm spheres produced small contrast reductions on the order of 0.005. These results are not directly comparable to the simulated results but do show that some contrast reduction was observed with the larger sphere diameters.

5.2 SIMULATION OF SEEDING EXPERIMENTS

A series of simulations were made to aid interpretation of the laboratory measurements. A volume scattering function was calculated for each particle diameter using a Mie code developed by Kattawar [1988] and a index of refraction of 1.60+0i. Calculated VSFs are shown in Figure 19 for six particle sizes. As expected the small particle sizes exhibit a broad peak. The larger the particle size the broader the small angle peak. Each of these VSFs was used to obtain a simulated trace of scattered photon energy on the linear detector array using the laboratory geometry. These simulations are shown in Figure 20 and indicate that at the fixed spatial frequencies of the experiment the contrast has decayed to the high frequency limit [e^{-1}] except at the larger particle size diameters. Thus, the simulation results are consistent with the laboratory observations.

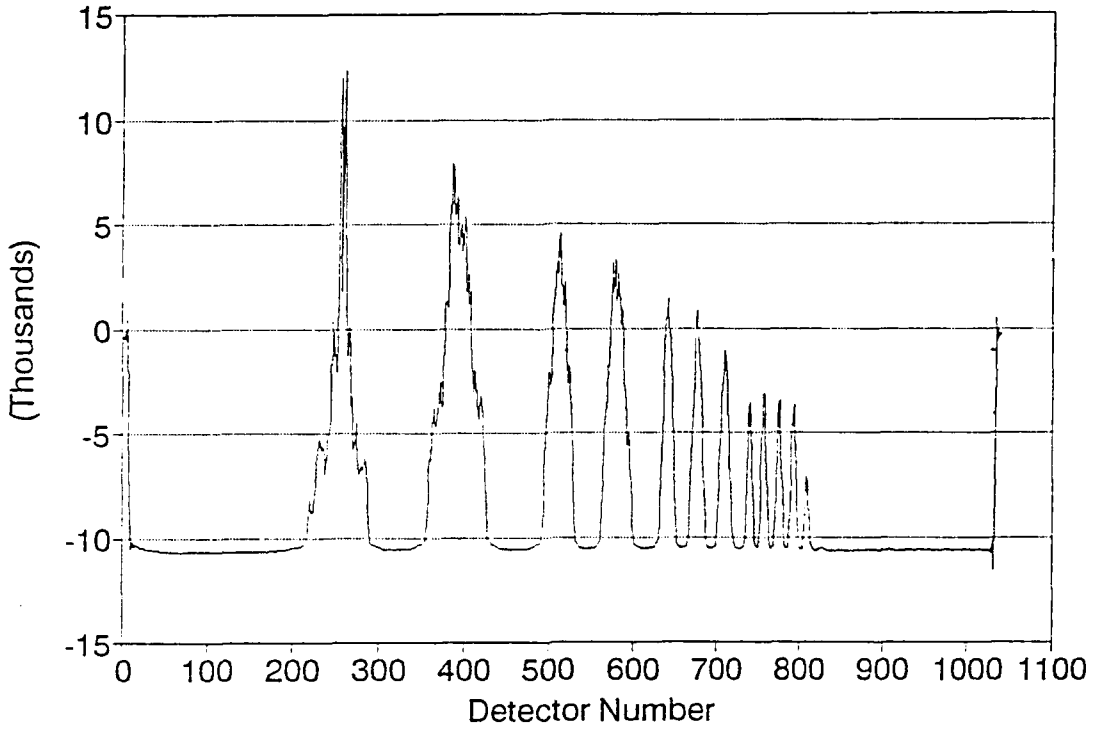

Figure 15. Scan of Linear Detector Array in the Seeding Experiments With 2.92 Micron Particles

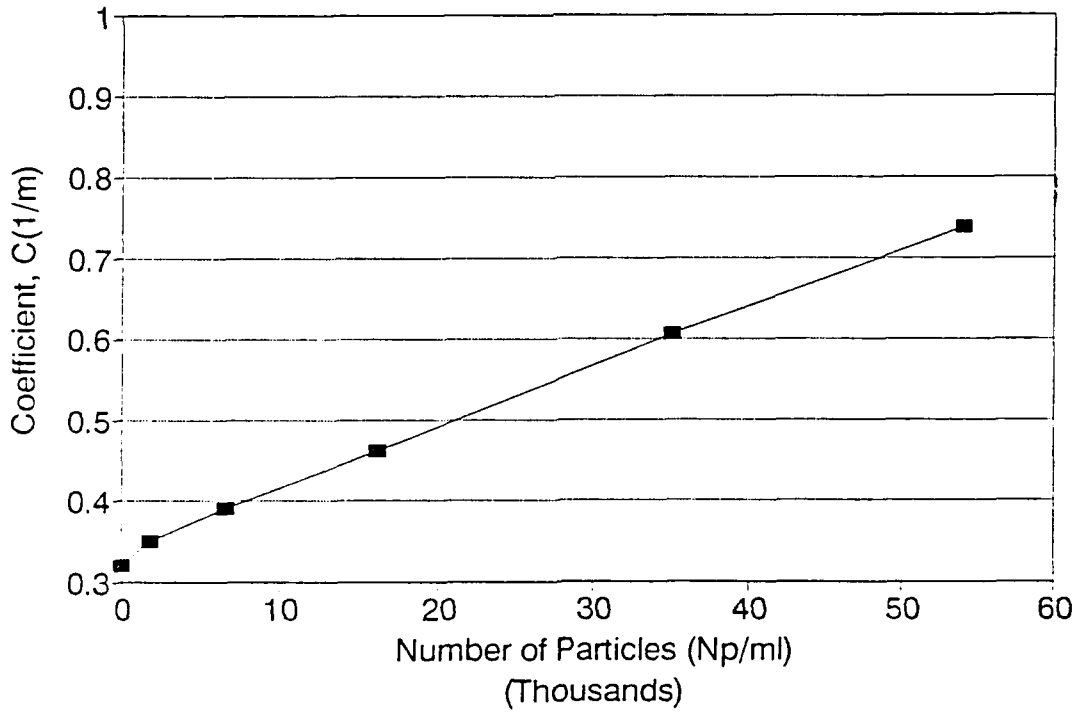

Figure 16. Beam Attenuation Measurements Versus Number of 2.92 Micron Polystyrene Particles

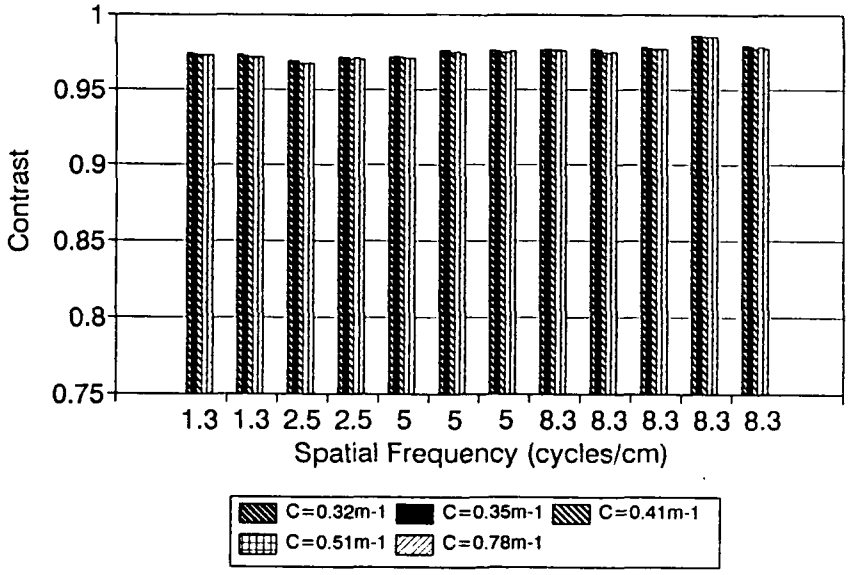

(a)

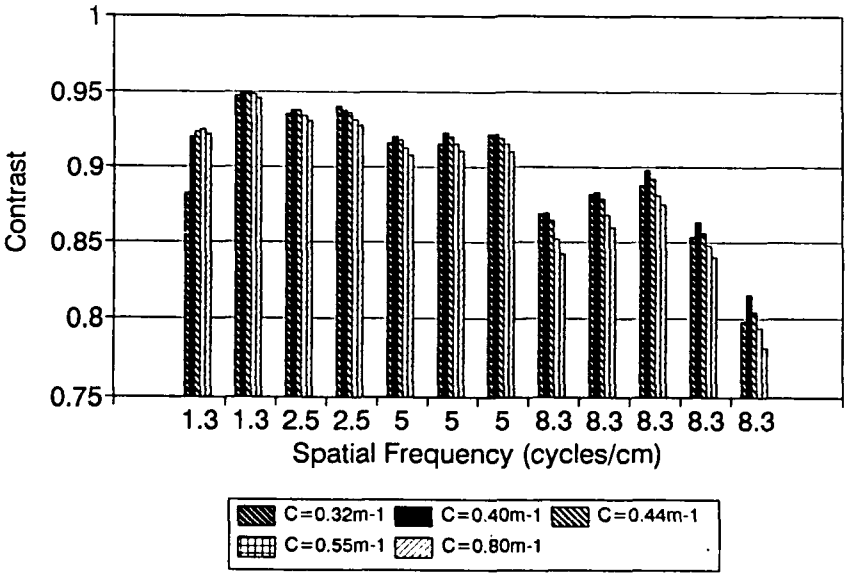

(b)

Figure 17. Estimated Contrasts (Difference/Sum) at Spatial Frequencies Recorded for the (a) 0.49 Micron Spheres and (b) 0.99 Micron Spheres

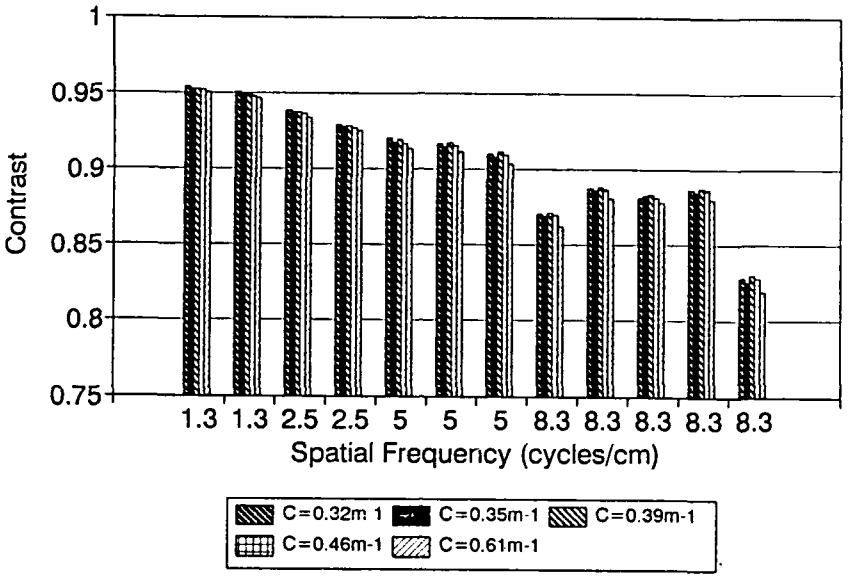

(a)

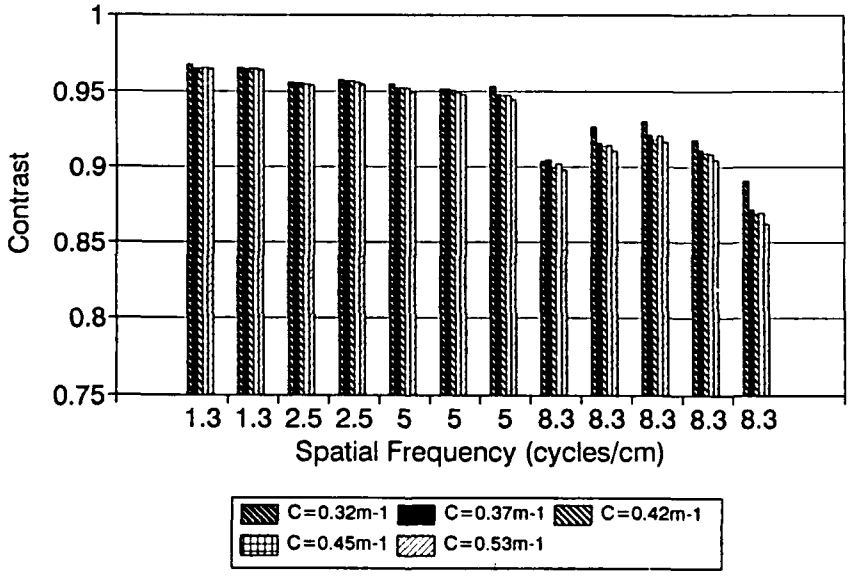

(b)

Figure 18. Estimated Contrasts (Difference/Sum) at Spatial Frequencies Recorded for the (a) 2.92 Micron Spheres and (b) 25.0 Micron Spheres

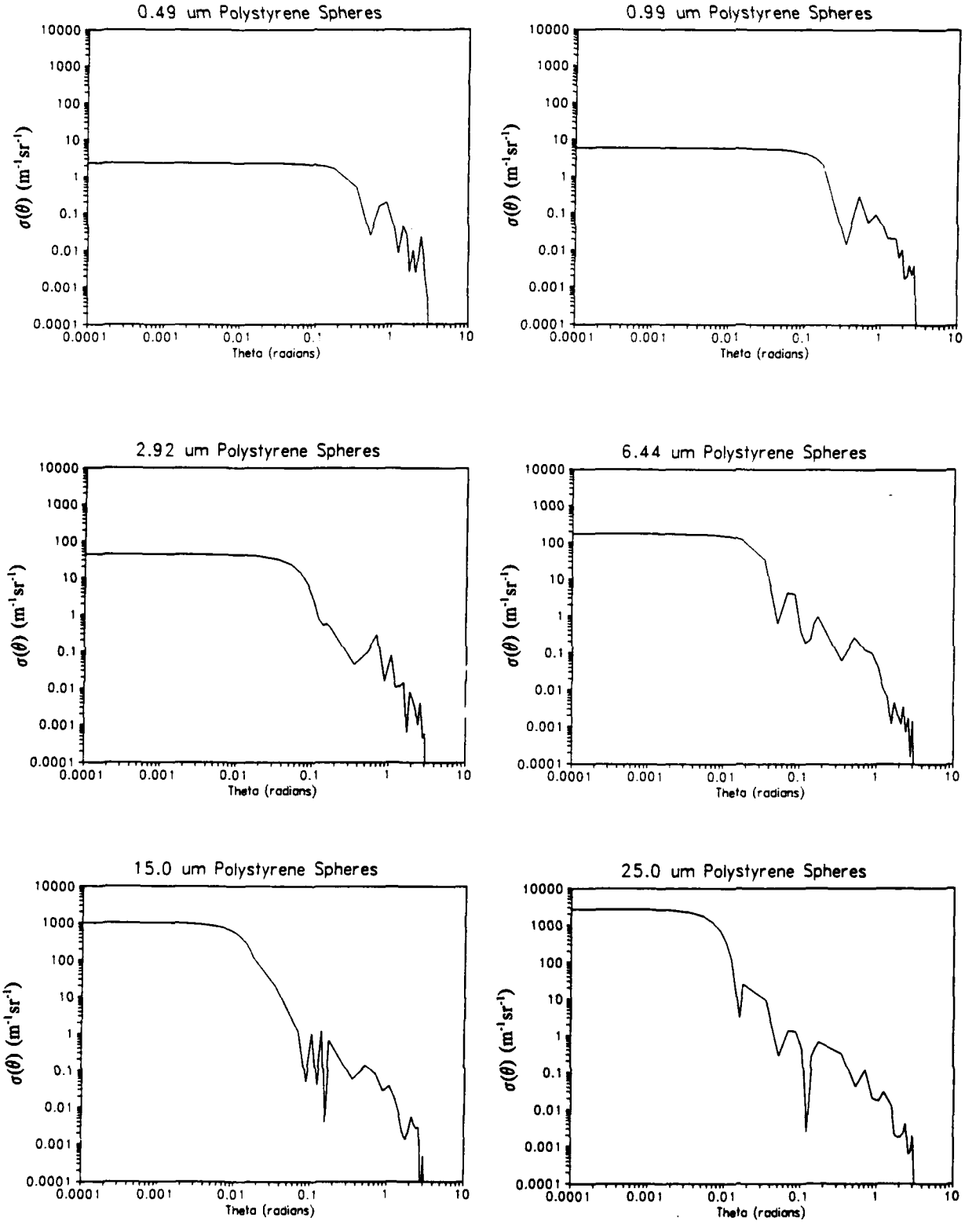

Figure 19. Volume Scattering Functions Calculated With Mie Theory Particle Diameters From 0.49 μm to 25.0 μm and a Refractive Index of 1.60 + 0i λ = 633 nm

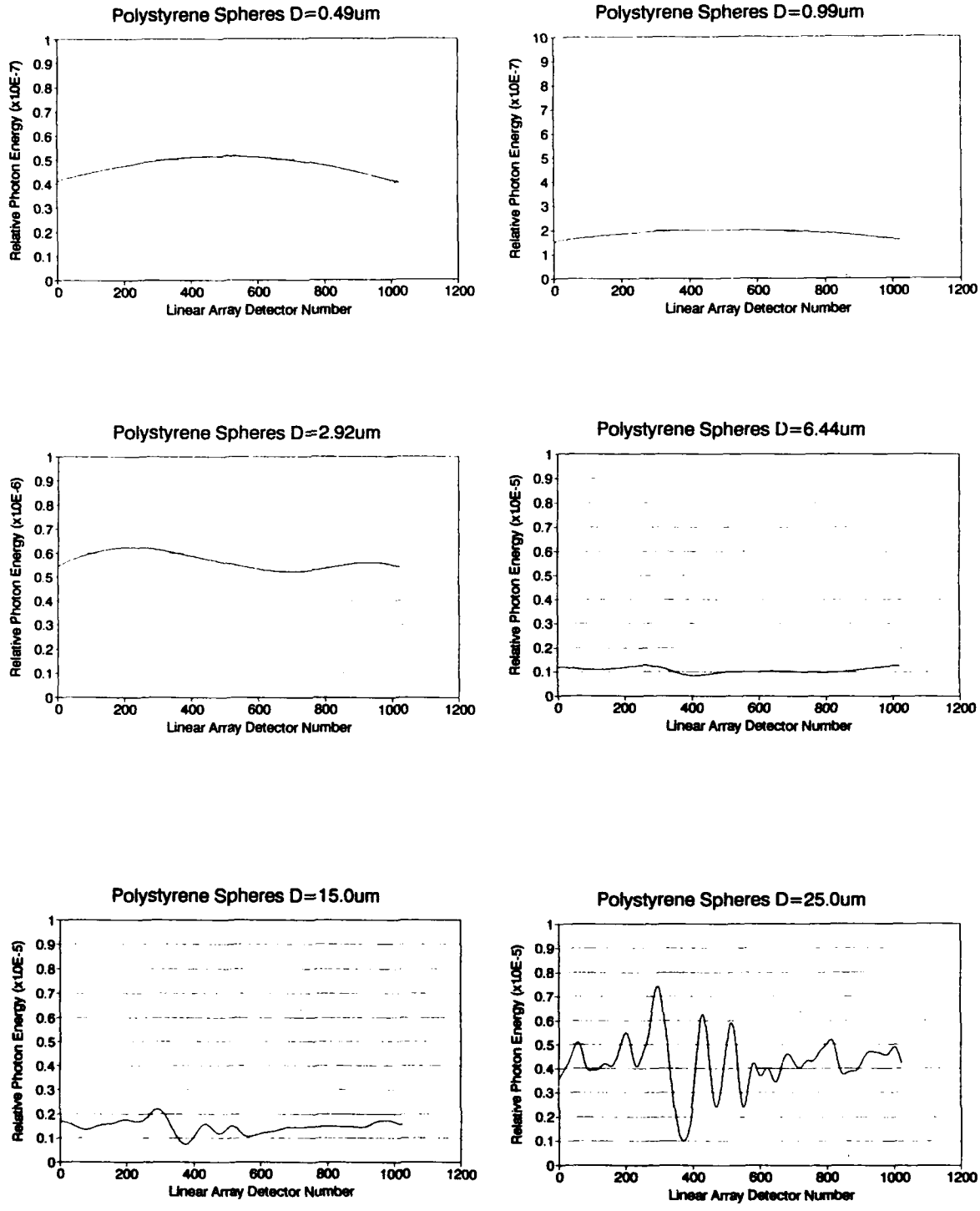

Figure 20. Simulated Scattered Energy Received on Linear Detector Array for a Path Length of 41 cm and a Beam Attenuation of 0.2 m^{-1}

5.3 SIMULATION OF AUTEC WATER

The performance of the holographic small angle scattering meter was investigated for natural waters using the sensor simulator and the AUTEC volume scattering function. The 25cm path instrument was simulated for each of two scattering functions shown in Figure 21 where the VSF1 is the original scattering function and VSF2 is a modified function with small angle scattering reduced by approximately a factor of ten. The derived MTF for each of these functions is shown in Figure 22 along with the simulated measurements. The simulated patterns of scattered energy on the detector array for VSF1 and VSF2 from which contrasts were calculated is shown in Figure 23a. The MTF1 function was previously parameterized (see Figure 5). This parameterization was used to refit MTF1 based upon the simulated measurement data. In this procedure the previously derived $f_1(\psi)$ is held constant while the α parameter in $f_2(\psi)$ is allowed to vary until a least squares fit is obtained with the measurement data. An α value of 0.3016 was obtain for the fitted function shown in Figure 22. The simulated measurements made using VSF2 are shown in Figure 24. The MTF1 function and parameterization, for this demonstration, can be considered to be the standard. The simulated measurements made with VSF2 were then used in combination with the standard MTF parameterization to derive an estimate of MTF2 also shown in Figure 24. The derived MTF appears to be a good fit to the measurement points which lie slightly above the MTF2 curve. In the last step this derived MTF was inverted to estimate the small angle scattering function for VSF2 as shown in Figure 25. The resulting scattering function lies slightly above VSF2 as would be expected based upon the relationships between the MTFs given previously in Figure 24. In another exercise an attempt was made to derive the MTF for the 25.0 micron particles and compare the results to simulated and laboratory measurements. The MTF of the original VSF for these particles could not be

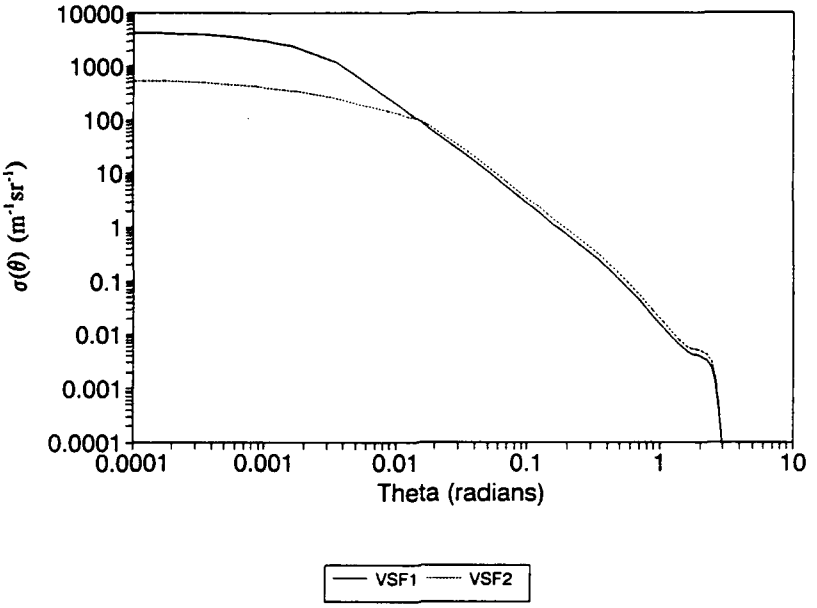

Figure 21. Volume Scattering Function for AUTEC Sample Number 7 (VSF1) and a Modified Version With Small Angle Scattering Reduced by Approximately 10x (VSF2)

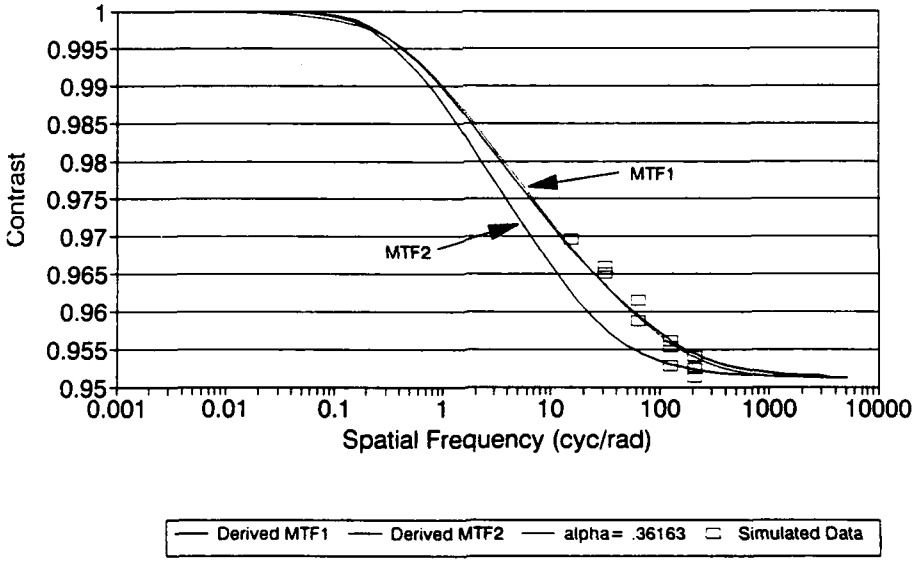

Figure 22. Derived Modulation Transfer Functions for AUTEC Number 7 (MTF1) and for VSF2 (MTF2) Using a 25 cm Instrument Sample Path Length and C=0.2 m^{-1}. The Dotted Curve With α = .3616 was Fitted to MTF1 Using the Simulated Measurements

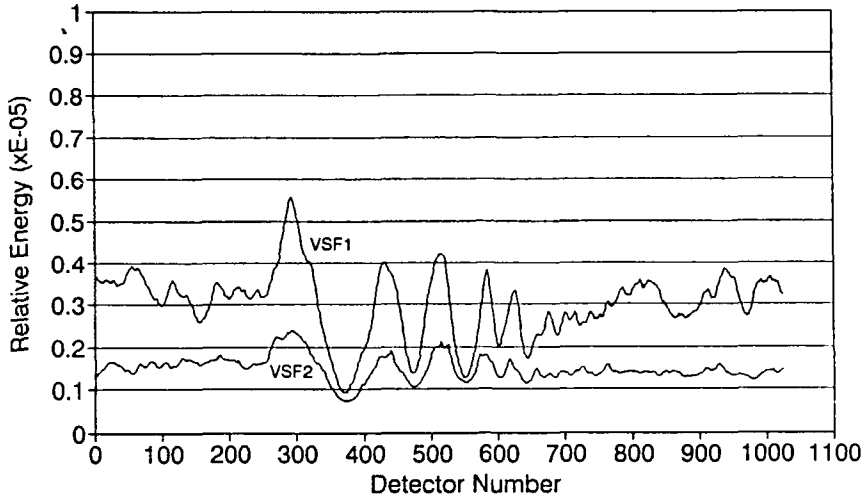

(a)

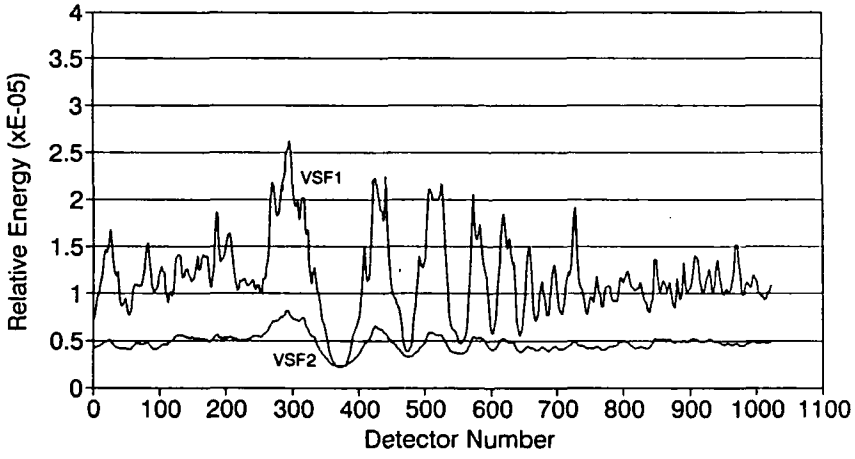

(b)

Figure 23. Simulated Distribution of Scattered Energy on the Linear Detector Array Using Volume Scattering Functions VSF1 and VSF2. Panel (a), Path Length = 25 cm, C = 0.2 m^{-1} Panel (b) Path Length = 100 cm, C = 0.2 m^{-1}

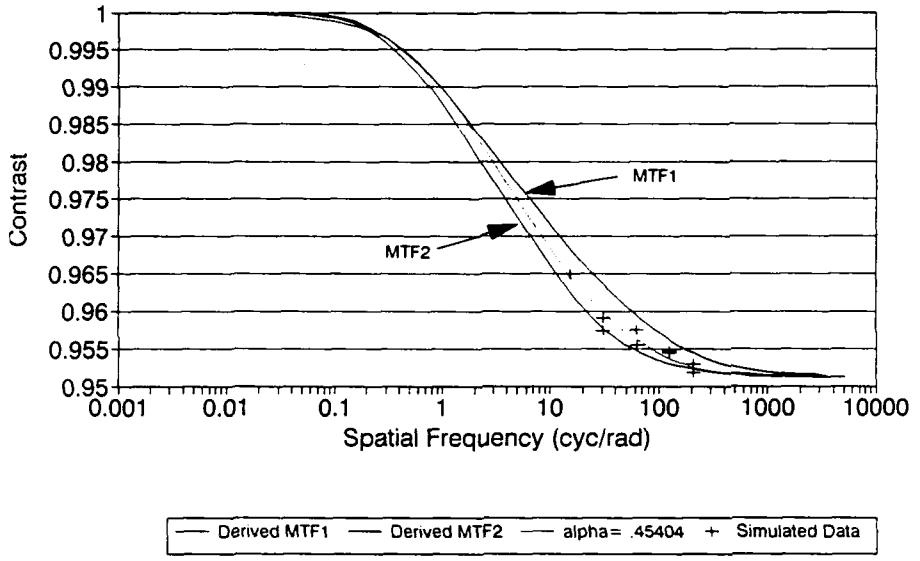

Figure 24. Derived MTF (Dotted Curve) Based Upon Simulated Measurements Made Using VSF2

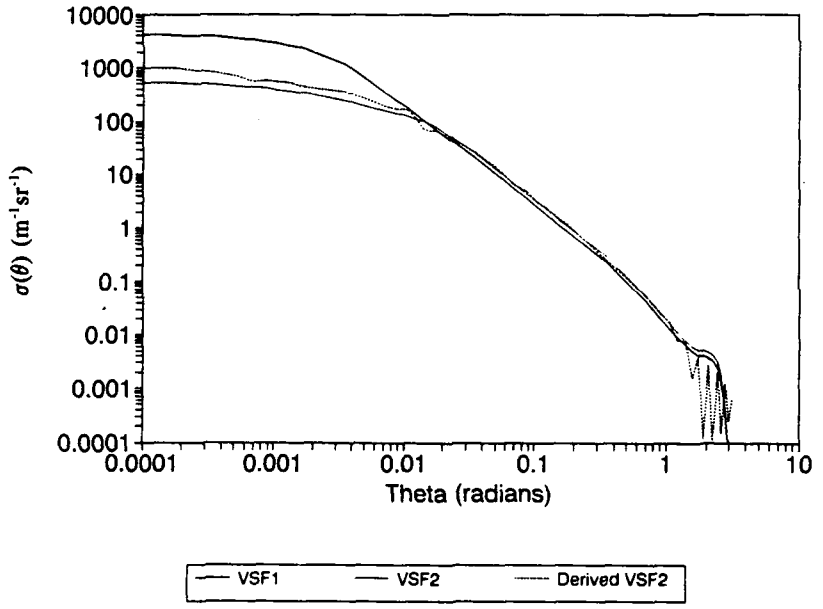

Figure 25. Volume Scattering Functions for MTF1, MTF2, and Derived VSF Based Upon the Simulated Measurements Using VSF2 and the MTF1 Parameterization

calculated because of the large lobes in the scattering function. As an alternative this VSF was fitted with a smooth curve as shown in Figure 26 suitable for MTF conversion. The resulting MTF is plotted in Figure 27 together with both the laboratory measurements and the simulated measurements. The laboratory measurements are uncalibrated and therefore are not directly comparable to the simulated data but do appear to have a comparable decay relationship with spatial frequency.

5.4 DISCUSSION OF RESULTS

The results from the experiments and simulations are encouraging and support the holographic MTF measurement concept for small angle scattering. Obviously more quantitative measurements are needed and more complete simulations made which incorporate detector noise and instrument drift. These considerations are especially important to simulating instrument performance tradeoffs with path length. In the present simulations nearly perfect resolution of scattered plus direct energy was assumed. The simulated pattern of scattered energy on the detector array shown in Figure 23b appear noisy because the simulation times were insufficient to sample all the multiple scattering effects with the longer one meter path length. Patterns of scattered energy for 25cm and 100cm path lengths otherwise appear quite similar and the demonstrated measurement capability above could be expected to be comparable independent of path length. For the present simulations for Tongue of the Ocean waters the ratio of scattered energy to direct in a 25cm instrument with a 1024 element array is about 1:500. In a one meter instrument this ratio becomes 1:95 and in a four meter instrument 1:16. This ratio also represents a reasonable lower limit for the SNR resulting from a combination of hologram and detector noise. In the present laboratory demonstration a SNR of 100:1 was achieved and extensive

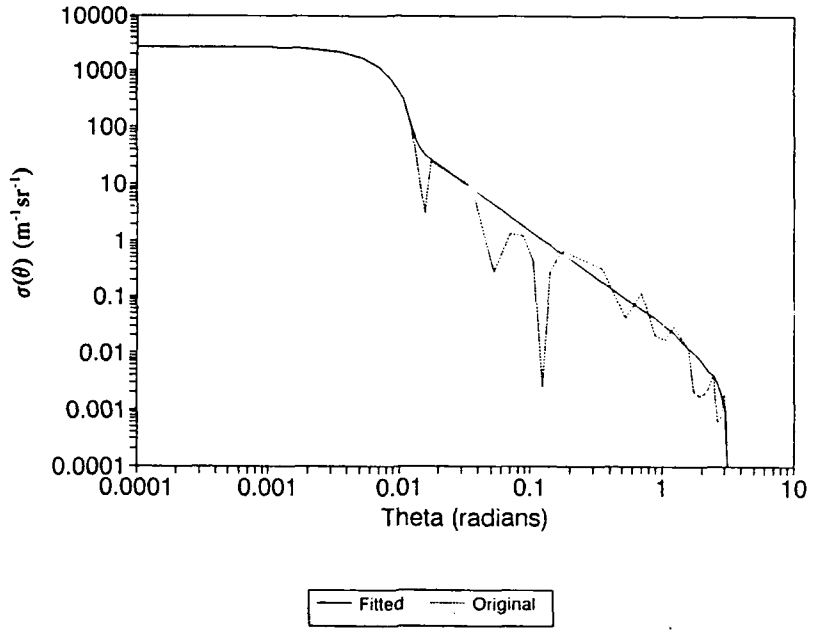

Figure 26. Volume Scattering Function for 25. 0 μm Particles and Fitted Smooth Curve

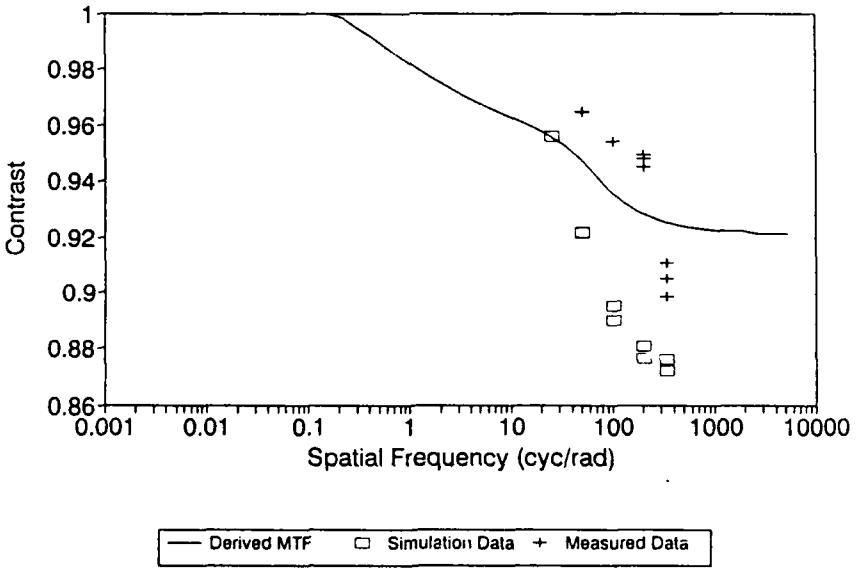

Figure 27. Comparison of Derived MTF From the Fitted Function for 25.0 μm Particles With Simulated and Laboratory Measurements

averaging was therefore required to reduce the effects of noise. The hologram speckle noise is likely to be limiting in a practical instrument. However, a hologram SNR between 500:1 and 1000:1 is achievable.

6.0 CONCLUSIONS AND RECOMMENDATIONS

A preliminary design concept has been developed for a holographic instrument to measure scattering and transmission optical properties of ocean waters. Use of holographic optics allows compact integration needed in an expendable unit. The laboratory experiments and simulations demonstrate that a holographic MTF instrument is feasible and will provide valuable small angle measurements.

It is recommended that this basic research continue and be directed towards the following goals.

1. Develop methodology to construct a lenslet hologram needed for a multiple path transmissiometer and to integrate with the hologram needed for the MTF small angle meter.

2. Develop recording techniques to construct needed holograms with SNR values in excess of 500:1.

3. Develop complete calibrations techniques for the MTF meter and conduct laboratory measurements with poly-dispersions characteristic of oceanic waters.

4. Develop simulations for the transmissometer, large angle scatterometer, and backscatter meter. Compare results with theoretical models and measurement data.

5. Develop a complete integrated concept design which includes all measurement functions.

After completion of the concept design phase the project can be transferred to a Phase I prototype design which will involve fabrication of a retrievable instrument. Laboratory and tank tests will be conducted to evaluate accuracy and stability. Phase II, prototype evaluation will involve participation in a series of Navy ocean optics cruises. During this phase an advanced prototype instrument will be developed which

includes the XBT wire launch technology. During Phase III, advanced prototype development, multiple retrievable units will be develop and an extensive evaluation program will be conducted.

7.0 REFERENCES

Austin, R.W., and T.J. Petzold, An Instrument for the Measurement of Spectral Attenuation Coefficient and Narrow Angle Volume Scattering Function of Ocean Waters, SPIE, vol. 64, Ocean Optics I, 1975.

Bracewell R. N., The Fourier Transform and Its Applications, Second Edition, McGraw Hill, 1986.

Del Grosso, V.A., Modulation Transfer Function of Water, SPIE, vo. 64, Ocean Optics I, 1975.

Kattawar, G.W., Personal Communication, 1988.

Petzold, T.J., Volume Scattering Functions for Selected Ocean Waters, Scripps Institution of Oceanography, University of California, SIO ref. 72-78, October 1972.

Tanis, F.J., G.W. Kattawar, and G.D. Hickman, Influence of Scattering on the Diffuse Attenuation Coefficient in the Asymptotic Region, SPIE vol. 637, *Ocean Optics VIII*, 1986.

Upatnieks J., Compact Holographic Sight, SPIE vol. 883, Holographic Optics: Design and Applications 1988.

Wells, W. H., Loss of Resolution in Water as a Result of Multiple Small Angle Scattering, J. Opt. Soc. Am., v. 59, p. 686, June 1969.

Wells, W. H., Theory of Small Angle Scattering, AGARD Paper No. 61, 1973

Zaneveld, R.V., and R. Bartz, Beam Attenuation and Absorption Meters, SPIE vol. 489, Ocean Optics VII, 1984.